

Anomalously strong polarization dependence of the intensity of magnetically-induced atomic transitions

ARMEN SARGSYAN¹, EMMANUEL KLINGER^{2,*}, AREVIK AMIRYAN¹, AND DAVID SARKISYAN¹

¹Institute for Physical Research – National Academy of Sciences of Armenia, 0204 Ashtarak-2, Armenia

²Institut FEMTO-ST – UMR 6174 CNRS, SupMicroTech-ENSMM, Université de Franche-Comté, 25030 Besançon, France

* Corresponding author: emmanuel.klinger@femto-st.fr

Compiled June 25, 2024

The impact of the optical field polarization on the spectrum of magnetically-induced transitions, a class of transitions forbidden at zero magnetic field, is studied with a weak-probe sub-Doppler technique. The high spectral resolution of the technique combined with the simplicity in interpreting the observed spectra, allows to follow the behavior of individual transitions as a function of the magnetic field amplitude. We observe only one intense transition (out of $2F_g + 1$) in the case of linear (π) polarization in the $F_g \rightarrow F_g + 2$ manifolds of ^{85}Rb , ^{87}Rb and ^{133}Cs for fields above a few hundreds of gauss. We show that this behavior is in agreement with a model based on the diagonalization of the Zeeman Hamiltonian matrix. With the rapid development of micro-machined vapor-cell-based sensors these results will be of use to magnetometers operating above Earth field, wide-range laser frequency stabilization systems and atomic Faraday filters. © 2024 Optica Publishing Group

<http://dx.doi.org/10.1364/ao.XX.XXXXXX>

Optical and magneto-optical processes formed in hot atomic vapors of alkali metal atoms are at the core of many devices and applications, such as atomic optical clocks and gyroscopes [1], optical magnetometers [2], frequency markers of atomic transitions [3], realization of narrow optical resonances based on coherent processes [4], sensitive sensors of electric and microwave fields based on Rydberg atoms [5], etc. Therefore, the identification of new intense atomic transitions of alkali metals is of great interest.

The Zeeman effect occurs when atoms are in the presence of an external magnetic field, leading to a significant modification of the intensity of atomic transition [6, 7]. One interesting consequence of the couplings between magnetic sub-levels induced by the Zeeman effect is the possibility to observe transitions with an apparent $\Delta F = \pm 2$ selection rule at non-zero field. These transitions, referred to as magnetically-induced (MI) transitions, form a large class of one hundred transitions with interesting and important features [8–10]. Interest in these transitions is primarily driven by the fact that, in wide ranges of magnetic fields, their intensities can significantly exceed the intensities of “usual” (i.e. $\Delta F = 0, \pm 1$), widely used atomic transitions. In

addition, their frequency shifts in strong magnetic fields reach 20 to 30 GHz, enabling the exploration of new frequency ranges for the frequency stabilization of lasers operating at significantly shifted frequencies compared to unperturbed atomic transitions. These transition can also be used to form coherent processes such as electromagnetic-induced transparency in large magnetic fields [11, 12]. A thorough understanding of the evolution of alkali transitions in a magnetic field is also important for magnetometry above Earth field [13, 14].

Despite possessing interesting features, magnetically-induced transitions are often disregarded because traditional weak-probe spectroscopy lacks the resolution to distinguish individual transitions due to the Doppler effect. Conversely, sub-Doppler spectra acquired through nonlinear techniques, such as saturated absorption, is cumbersome to interpret because of the large number of transitions [15]. However, with nanocells (NCs), where the vapor is confined between two almost-parallel windows separated by a distance ranging from a few nm to several μm , one can realize weak-probe sub-Doppler spectroscopy [16]. By selecting the proper cell thickness, this can be used to realize sub-Doppler spectroscopy of molecular lines [17]. Beyond spectroscopy, NCs serve as a crucial tool in fundamental physics. They are, for instance, used to study atom-surface interactions [18–20], cooperative effects [21], and realize single-photon generation at room temperature [22]. New advancements in manufacturing techniques [23] are making nanocells (NCs) increasingly accessible.

In this article, we study the evolution of MI transitions of Rb and Cs vapors, confined in a NC, in the presence of a magnetic field. To improve the resolution of the measurement, second derivative spectroscopy [24, 25] is used. We show that the spectrum of $F_g \rightarrow F_g + 2$ MI transitions excited under linearly-polarized (π) optical field contains only one intense transition out of $2F_g + 1$. In contrast, the spectrum of $F_g \rightarrow F_g + 2$ MI transitions excited under circularly-polarized (σ^+) optical field contains $2F_g + 1$ intense transitions, that is 3 transitions for ^{87}Rb , 5 transitions for ^{85}Rb , and 7 transitions for ^{133}Cs .

In the presence of a magnetic field, magnetic sublevels are split and mixed, leading to changes in transition probabilities and frequencies. These changes can be calculated by diagonalizing the Hamiltonian matrix [6], which accounts for the hyperfine

atomic structure, and the Zeeman Hamiltonian, that is

$$H = H_{\text{hfs}} + \frac{\mu_B}{\hbar} (g_S S_z + g_L L_z + g_I I_z) B_z, \quad (1)$$

where μ_B is the Bohr magneton [26], $g_{S,L,I}$ are the Landé factors [27] and S_z, L_z, I_z the projection of quantum numbers on the z -axis (quantization axis). The eigenvalues obtained after the diagonalization of the matrix provide access to the resonance frequencies. The transition intensities are proportional to the squared dipole moment, given by

$$| \langle e | d | g \rangle |^2 \propto \Gamma_N a^2 [\psi(F'_e, m_{F'_e}); \psi(F'_g, m_{F'_g}); q], \quad (2)$$

where Γ_N the natural linewidth of the transition, $a [\psi(F'_e, m_{F'_e}); \psi(F'_g, m_{F'_g}); q]$ are the transfer coefficients modified by the field [6], calculated using the eigenvectors. Here, $q = 0, \pm 1$ is associated with the polarization of the incident laser field. To excite π ($q = 0$) transitions, the polarization of the electric field of the laser should be collinear with the applied magnetic field axis.

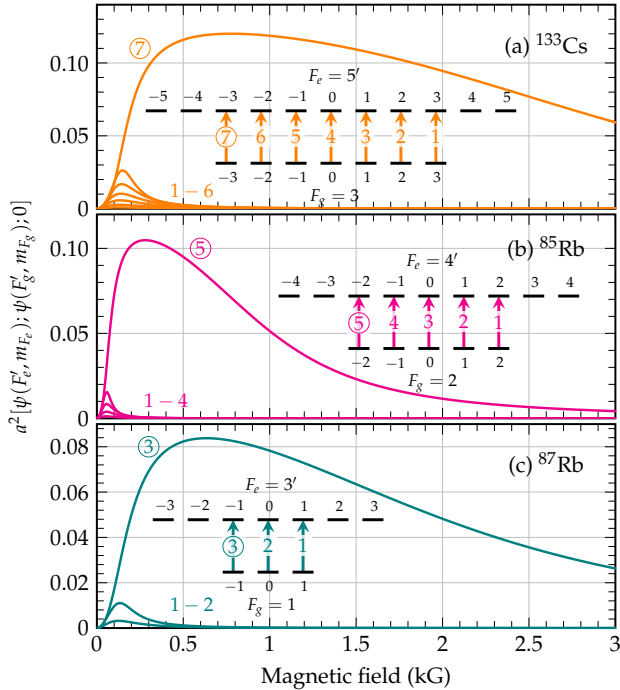


Fig. 1. Dependence of the intensity of (a) ^{133}Cs , (b) ^{85}Rb and (c) ^{87}Rb $F_g \rightarrow F_g + 2$ MI transitions versus magnetic field when excited by linear π -polarization. In large magnetic fields, atoms are left with only one MI transition (out of $2F_g + 1$). In each plot, the inset shows the diagram of transitions with the corresponding labels.

Figure 1 shows the calculated evolution of $F_g \rightarrow F_g + 2$ MI transitions of the D_2 line of ^{133}Cs (a), ^{85}Rb (b) and ^{87}Rb (c) under π optical excitation. A rapid increase of the MI transition intensities can be seen as a function of the magnetic field for all three atoms. The characteristic magnetic field¹ $B_0 = A_{\text{hfs}}/\mu_B$, where A_{hfs} is the magnetic dipole constant of the ground state, is a good indicator for the dynamics of transitions. For each atom, one transition is seen to have a much larger increase in intensity, reaching a maximum at about $B \sim 0.5B_0$. With a further increase

¹ B_0 is 0.7 kG, 2.4 kG and 1.7 kG for ^{85}Rb , ^{87}Rb and ^{133}Cs , respectively.

of the magnetic field, the intensity smoothly decreases to almost zero. Note that a field $B \gg B_0$ marks the onset of the hyperfine Paschen-Back regime [28]. These transitions are labeled ③, ⑤, ⑦, for ^{87}Rb , ^{85}Rb and ^{133}Cs , respectively, see the insets in Fig. 1. Conversely, the intensities of all other transitions quickly tend to zero for fields $B > 0.2B_0$. Thus, in magnetic field above $0.2B_0$, only one $\Delta F = +2$ transition remains in the spectrum of alkali D_2 line observed under π -polarization. Qualitatively, this behavior can be explained as follows: the excitation by linear π -radiation can be represented as an excitation by a coherent superposition of σ^+ and σ^- polarized light. When excited by σ^- -polarization, only one MI transition remains in the spectrum [28]. The excitation by π -polarized radiation is then dominated by the σ^- part and only one intense MI transition can be observed. Note that our calculations also show that $\Delta F = -2$ atomic transitions formed in strong B -fields with π -polarization are much weaker in intensity than for $\Delta F = +2$ transitions. For this reason, we focus only on the latter.

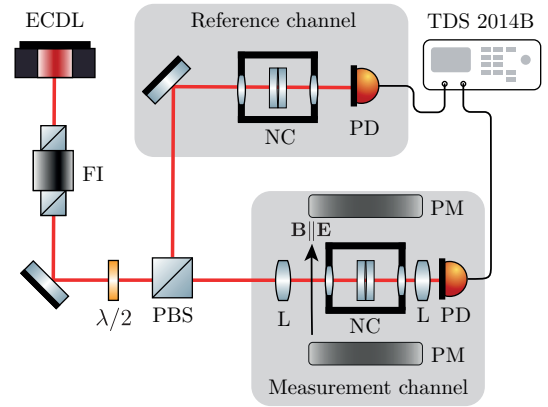


Fig. 2. Sketch of the experimental setup. ECDL – extended cavity diode laser, FI – Faraday isolator, PBS – polarizing beam splitter, L – lens, PM – permanent magnet, NC filled with Rb or Cs in the oven, PD – photodiodes. The PMs are oriented such that applied magnetic field B is collinear with the electric field of the laser radiation E ($B \parallel E$) in order to excite π transitions. The reference channel comprises a Rb (or Cs) nanocell from which the transmission spectrum of the D_2 line is recorded at zero magnetic field.

The sketch of the experimental setup is shown in Fig. 2. A linearly-polarized laser beam, emitted by a cw extended cavity tunable diode laser (ECDL) [29] is used. When the experiments is carried out with Rb atomic vapor, an ECDL with $\lambda = 780$ nm is tuned in the vicinity of the Rb D_2 line. In the case of Cs atomic vapor, another ECDL with $\lambda = 852$ nm, is tuned in the vicinity of the Cs D_2 line. In both cases, the spectral width of the probe laser radiation is $\gamma_l < 1$ MHz. In order to avoid feedback in the cavity, a Faraday isolator is placed immediately after the laser. A polarizing beam splitter (PBS) is used to purify the initial linear optical polarization and direct part of the light to an auxiliary channel serving as a frequency reference. The laser fields transmitted through NCs in both the measurements and reference channels are detected by a photodiode and the signal fed to a Tektronix TDS 2014B digital four-channel oscilloscope.

To excite π transitions, the applied magnetic field should be collinear with the polarization of the incident laser field, i.e. $B \parallel E$. To apply fields above 0.5 kG, a set of two strong permanent magnets mounted on a translation stage was used. The

magnetic field strength applied to the atomic vapor is varied via a simple longitudinal displacement of the PM set [30], calibrated with a Teslometer HT201 magnetometer. Because, in this configuration, the field is applied along the long side of the nanocell with PMs, a high gradient is also introduced and not mitigated as in the case of σ^\pm excitations [13]. This results in an additional broadening of the transitions. To form the narrowest resonance possible, the spectroscopy is performed at a vapor column thickness of $\ell = \lambda/2$ [16]. The laser beam diameter is reduced down to ~ 1 mm to only illuminate a region where ℓ is homogeneous. The acquired spectra are then post-processed with second derivative (SD). The resulting spectrum $T''(\nu)$ typically shows transitions with spectral linewidth of $\sim 20 - 30$ MHz, which is narrower by a factor of ~ 20 compared with the Doppler broadening. This allows to separate and study atomic transitions individually. Note that the SD method correctly shows the relative intensities of atomic transitions and their frequency positions, it can therefore be used for quantitative measurements [25].

Figure 3 shows the experimental (black dots) SD transmission spectrum obtained using a NC filled with natural-abundance Rb atomic vapor at a column thickness $\ell = 390$ nm and a field $B = 800$ G, upon excitation by a π -polarized radiation. It was recorded with a laser power of $20 \mu\text{W}$, and a NC temperature of 120°C . The laser frequency is scanned across the ^{85}Rb $F = 2 \rightarrow 3', 4'$ and ^{87}Rb $F = 1 \rightarrow 2', 3'$ manifolds of the D_2 line. The red solid line corresponds to the theoretical SD spectrum, calculated by second order numerical differentiation of the transmission spectrum. The theoretical transmission spectrum is obtained by summing the contribution of all possible transitions j , each of which is treated as an independent two-level system:

$$T(\nu) \propto \frac{1}{|Q|^2} \cdot \sum_j \text{Im} [\chi_j(\nu, \ell, B)], \quad (3)$$

where $Q = 1 - r^2 \exp(2ik\ell)$, r is the (field) reflection coefficient of the cell windows. The two-level system lineshape $\chi_j(\nu, \ell, B)$, derived in Ref. [31], is a function of the cell thickness ℓ and the laser frequency ν ; it reads

$$\chi_j(\nu, \ell, B) = -4(1 - r \exp[ik\ell])^2 \cdot \frac{\sin^2(k\ell/2)}{Q} \cdot \frac{\mathcal{N}}{ku\sqrt{\pi}} \cdot \frac{iA_j(B)}{\Gamma/4\pi - i\Delta_j(B)}, \quad (4)$$

where \mathcal{N} is the vapor density, $u(\Theta) = \sqrt{2k_B\Theta/m_a}$ is the thermal velocity at a temperature Θ for atoms of mass m_a . The transition parameters $\Delta_j(B) = \nu - \nu_j(B)$ and $A_j(B)$ are fed from the results obtained after diagonalization of the Hamiltonian matrix, see Eq. (1). The homogeneous broadening Γ , including contributions from natural linewidth, collisional broadening, etc., is left as a free parameter in our simulations. As seen in Fig. 3, only one MI transition can be observed for each atom: $\textcircled{5}$ for ^{85}Rb and $\textcircled{3}$ for ^{87}Rb . In similar conditions, $2F_g + 1$ transitions have been observed in the case of σ^+ -polarized excitation [32]. Such a strong difference in the number of MI transitions excited when using σ^+ and π -polarizations is a manifestation of an anomalously strong polarization dependence of the intensity of transitions. Other nearby transitions belong to the ^{85}Rb $F = 2 \rightarrow 3'$ and ^{87}Rb $F = 1 \rightarrow 2'$ manifolds. A good agreement between the experiment and the theory can be observed. Nevertheless, some discrepancies can be seen which are likely due to laser instability during the measurements.

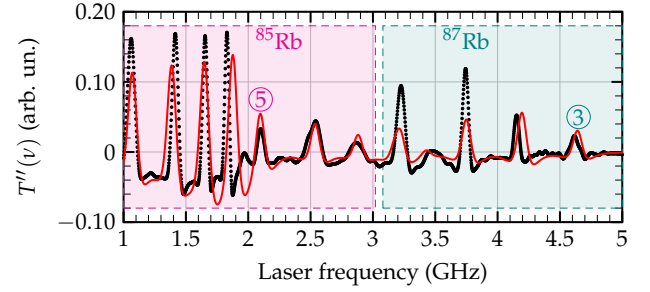


Fig. 3. Second derivative transmission spectrum recorded in the vicinity of the ^{85}Rb $F = 2 \rightarrow 3', 4'$ and ^{87}Rb $F = 1 \rightarrow 2', 3'$ manifolds. The experimental spectrum is obtained with a π -polarized excitation at $B = 800$ G and $\ell = 390$ nm. The red solid line represents the calculated spectrum. The weighted center of the ^{85}Rb D_2 line was chosen as the zero laser frequency. In this spectrum, only one MI transition remains at this field: transition $\textcircled{5}$ (out of a possible five, for ^{85}Rb), transition $\textcircled{3}$ (out of a possible three, for ^{87}Rb).

Figure 4 shows SD transmission spectra upon excitation by a linear π -polarized radiation, obtained from a Cs-filled NC at $\ell = 426$ nm and $B = 2.90$ kG (a), 1.95 kG (b) and 1.30 kG (c). For the experimental spectra (black dots), the laser is scanned in the vicinity of the D_2 line $F = 3 \rightarrow 3', 4', 5'$ transitions with a power of $30 \mu\text{W}$. The NC temperature is set to 100°C . As the theory predicts, there remains only one MI transition at these magnetic fields, the transition labeled $\textcircled{7}$, out of the possible 7. The other visible transitions belong to the $F = 3 \rightarrow 3', 4'$ of the Cs D_2 line manifold. Note that seven MI transitions have been observed in the case of σ^+ -polarized excitation in similar conditions [9]. As the magnetic field is increased above 1 kG, the intensity of the MI transition decreases. According to Fig. 1, the ratio of amplitude of the MI transition $\textcircled{7}$ at 1.30 kG to that at 2.90 kG should be about 1.8. However, on the spectra in Fig. 4, the observed ratio is about 2.7. This discrepancy is due to the increased transition broadening because of the magnetic field gradient from the PMs. The calculated spectra show a very good agreement with the experimental ones. To match, the broadening $\Gamma/2\pi$ in Eq. (4) had to be increased from 150 to 210 MHz. Note that the SD transmission spectrum is about 2.5 times narrower than the transmission spectrum given by Eq. (3).

In conclusion, we have studied the evolution of $F_g \rightarrow F_g + 2$ MI transitions of Rb and Cs D_2 lines, in the presence of a magnetic field upon linear π excitation. In the case of π excitation, the applied magnetic field is collinear with the laser polarization. In this configuration, the vapor is much more sensitive to the gradient produced by permanent magnets, which adversely leads the transition linewidth. This was partly overcome using weak-probe second derivative spectroscopy [16, 25], allowing individual atomic transitions to be resolved. For magnetic fields $B > 0.5B_0$, we predict and observe that only one MI transition (out of possible 3 for ^{87}Rb , 5 for ^{85}Rb and 7 for ^{133}Cs) remains in the spectrum. This is in contrast with the evolution of MI transitions in the case of circular σ^+ polarized excitation [9, 32]. Our calculations also show that such a feature exists for the MI transitions of all alkali atoms D_2 lines such as Na, K, Li, etc. Furthermore a similar feature is expected for $n^2S_{1/2} \rightarrow (n+1)^2P_{3/2}$ alkali lines, where $n = 3, 4, 5$ is the principal quantum number for Na, K, Rb respectively, which amounts to about 100 MI transitions [33]. With the rapid development of micro-machined

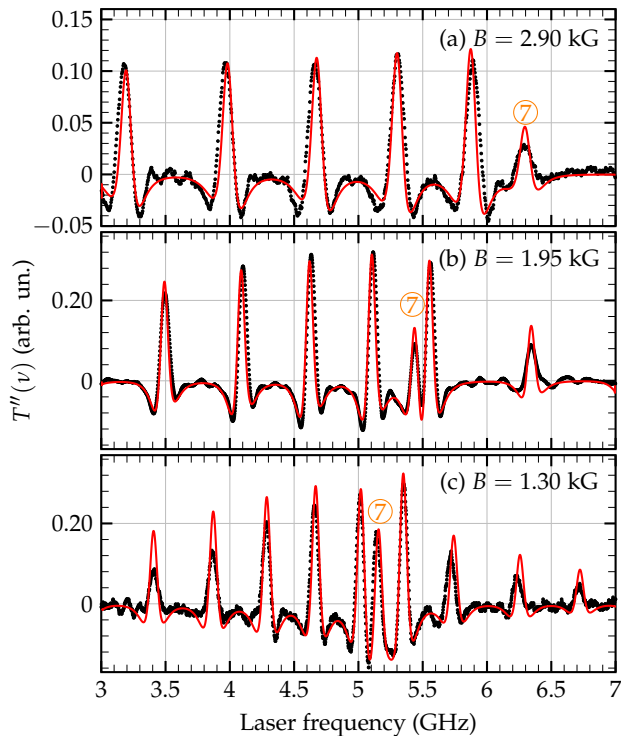


Fig. 4. Second derivative transmission spectrum recorded in the vicinity of the $F = 3 \rightarrow 4', 5'$ manifolds of the ^{133}Cs D_2 line. The experimental spectra are obtained with a π -polarized excitation, with $\ell = 426$ nm and $B = 2.90$ kG (a), 1.95 kG (b), 1.30 kG (c). The red solid lines represent the respective calculated spectra. The weighted center of the ^{133}Cs D_2 line was chosen as the zero laser frequency. In this spectrum, only one MI transition (out of a possible seven) remains at these fields: transition $\textcircled{7}$. The theory describes very well the frequency positions and amplitudes of the peaks.

vapor-cell-based sensors these results are important for magnetometers operating above Earth field, wide-range laser frequency stabilization systems and atomic Faraday filters.

FUNDING

The work was supported by the Science Committee of RA, in the frame of the research project No 21T-1C005.

ACKNOWLEDGMENTS

We thank Ara Tonoyan for fruitful discussions.

DISCLOSURES

The authors declare no conflicts of interest.

DATA AVAILABILITY STATEMENT

The data that support the findings of this study are available from the corresponding author upon reasonable request.

REFERENCES

1. J. Kitching, *Appl. Phys. Rev.* **5**, 031302 (2018).
2. A. Fabricant, I. Novikova, and G. Bison, *New J. Phys.* **25**, 025001 (2023).

3. D. Pizzey, J. D. Briscoe, F. D. Logue, *et al.*, *New J. Phys.* **24**, 125001 (2022).
4. R. Finkelstein, S. Bali, O. Firstenberg, and I. Novikova, *New J. Phys.* **25**, 035001 (2023).
5. L. A. Downes, L. Torralbo-Campo, and K. J. Weatherill, *New J. Phys.* **25**, 035002 (2023).
6. P. Tremblay, A. Michaud, M. Levesque, *et al.*, *Phys. Rev. A* **42**, 2766 (1990).
7. E. B. Alexandrov, M. P. Chaika, and G. I. Khvostenko, *Interference of atomic states*, vol. 7 (Springer, 1993).
8. A. Sargsyan, A. Amiryany, E. Klinger, and D. Sarkisyan, *J. Phys. B: At., Mol. Opt. Phys.* **53**, 185002 (2020).
9. A. Sargsyan, A. Amiryany, A. Tonoyan, *et al.*, *Phys. Lett. A* **390**, 127114 (2021).
10. A. Sargsyan, E. Klinger, A. Tonoyan, and D. Sarkisyan, *Optik* **303**, 171757 (2024).
11. A. Sargsyan, A. Tonoyan, A. Papoyan, and D. Sarkisyan, *Opt. letters* **44**, 1391 (2019).
12. A. Sargsyan, A. Amiryany, A. Tonoyan, *et al.*, *Phys. Lett. A* **434**, 128043 (2022).
13. E. Klinger, H. Azizbekyan, A. Sargsyan, *et al.*, *Appl. Opt.* **59**, 2231 (2020).
14. H. Stærkind, K. Jensen, J. H. Müller, *et al.*, *PRX Quantum* **5**, 020320 (2024).
15. S. Scotto, D. Ciampini, C. Rizzo, and E. Arimondo, *Phys. Rev. A* **92**, 063810 (2015).
16. G. Dutier, A. Yarovitski, S. Saliel, *et al.*, *Europhys. Lett.* **63**, 35 (2003).
17. G. G. Arellano, J. C. de Aquino Carvalho, H. Mouhanna, *et al.*, *Nat. Commun.* **15**, 1862 (2024).
18. A. Laliotis, B.-S. Lu, M. Ducloy, and D. Wilkowski, *AVS Quantum Sci.* **3**, 043501 (2021).
19. A. Sargsyan, R. Momier, C. Leroy, and D. Sarkisyan, *Phys. Lett. A* **483**, 129069 (2023).
20. B. Dutta, J. C. d. A. Carvalho, G. Garcia-Arellano, *et al.*, *Phys. Rev. Res.* **6**, L022035 (2024).
21. T. Peyrot, Y. R. P. Sortais, J.-J. Greffet, *et al.*, *Phys. Rev. Lett.* **122**, 113401 (2019).
22. F. Ripka, H. Kübler, R. Löw, and T. Pfau, *Science* **362**, 446 (2018).
23. T. Peyrot, C. Beurthe, S. Coumar, *et al.*, *Opt. Lett.* **44**, 1940 (2019).
24. W. Demtröder, *NASA STI/Recon Tech. Rep. A* **82**, 12273 (1981).
25. A. Sargsyan, A. Amiryany, Y. Pashayan-Leroy, *et al.*, *Opt. Lett.* **44**, 5533 (2019).
26. B. Olsen, B. Patton, Y.-Y. Jau, and W. Happer, *Phys. Rev. A* **84**, 063410 (2011).
27. H. Stærkind, K. Jensen, J. H. Müller, *et al.*, *Phys. Rev. X* **13**, 021036 (2023).
28. L. Weller, K. S. Kleinbach, M. A. Zentile, *et al.*, *J. Phys. B: At. Mol. Opt. Phys.* **45**, 215005 (2012).
29. V. Vassiliev, S. Zibrov, and V. Velichansky, *Rev. scientific instruments* **77**, 013102 (2006).
30. A. Sargsyan, G. Hakhumyan, C. Leroy, *et al.*, *Opt. letters* **37**, 1379 (2012).
31. G. Dutier, S. Saliel, D. Bloch, and M. Ducloy, *J. Opt. Soc. Am. B* **20**, 793 (2003).
32. E. Klinger, A. Sargsyan, A. Tonoyan, *et al.*, *The Eur. Phys. J. D* **71**, 216 (2017).
33. A. Tonoyan, A. Sargsyan, R. Momier, *et al.*, *Opt. Mem. Neural Networks* **32**, S343–S348 (2023).